Long-term thermal imbalance in large borehole heat exchangers array - A numerical study based on the Leicester project

Shuang Chen[a,b], Wanlong Cai[a,c], Francesco Witte[d], Xuerui Wang[e], Fenghao Wang[c], Olaf Kolditz[a,b], Haibing Shao[a,*]

[a] *Helmholtz Centre for Environmental Research - UFZ, Permoserstraße 15, 04318 Leipzig, Germany*
[b] *Faculty of Environmental Sciences, Dresden University of Technology, Germany*
[c] *School of Human Settlements and Civil engineering, Xi'an Jiaotong University, Xi'an, Shaanxi 710049 China*
[d] *Flensburg University of Applied Sciences, 24943 Flensburg, Germany*
[e] *Institute of mechanics and computational mechanics, University Hannover, Germany*

Abstract

When a Borehole Heat Exchanger (BHE) array is coupled with heat pump to provide cooling and heating to the buildings, thermal interaction between BHEs may occur in the subsurface. In the long term, imbalanced seasonal thermal load may lead to low or high temperature zones accumulating in the centre of the array. In this study, numerical models are configured according to a real BHE array project in Leicester, UK, and verified against monitoring data. Based on this reference model, a series of numerical experiments are conducted to investigate the response of circulation fluid temperature to different settings of imbalanced thermal load. It is found that over long-term operation, the sub array with a larger number of installed BHEs is shifting its thermal load towards the other branch with less BHEs installed. Within each sub array, the heat injection rate on the central BHEs is gradually shifted towards those located at the edge. A linear correlation is also found between the working fluid temperature increment and the amount of the accumulated heat injected into the subsurface.

Keywords: Shallow geothermal energy utilisation, Building heating and cooling, Borehole Heat Exchanger (BHE) array, Ground source heat pump, OpenGeoSys (OGS), Thermal Engineering System in Python (TESPy)

---

[*] Corresponding author
Email address: `haibing.shao@ufz.de` (Haibing Shao)

Nomenclature

Roman letters

b	wall thickness of pipe installed in the BHE (m)
c	specific heat capacity ($\mathrm{J\,kg^{-1}\,K^{-1}}$)
D	diameter of the BHE (m)
d	diameter of the pipe installed in the BHE (m)
k_s	roughness coefficient of the pipe (m)
L	length of the BHE (m)
l	length of the pipe (m)
$\dot{m}$	flow rate of the circulating fluid ($\mathrm{kg\,s^{-1}}$)
p	hydraulic pressure of the circulating fluid (bar)
$\dot{Q}$	heat extraction rate on the BHE (W)
Q	amount of heat (MWh)
Re	Reynolds number ($-$)
S	adjacent distance between BHEs (m)
T	temperature (°C)
t	time ($-$)
T_p	penalty temperature (°C)
V	volume of the BHE array ($\mathrm{m^3}$)
v	flow velocity in pipelines ($\mathrm{m\,s^{-1}}$)

Greek Letters

η	dynamic viscosity of circulating fluid (Pa s)
λ	thermal conductivity ($\mathrm{W\,m^{-1}\,K^{-1}}$)
π	mathematical constant Pi ($-$)

ρ density ($\mathrm{kg\,m^{-3}}$)

ζ Darcy friction factor as used in Eq. (1) ($-$)

Operators

Δ difference operator

$\int$ integral operator

Σ summation operator

Subscripts

f fluid

g grout

i index of BHE as used in Eq. (4)

in inlet pipe

ini initial time

out outlet pipe

p pipe

s solid or soil

Abbreviations

1U single U-shape pipe

BHE borehole heat exchanger

COP coefficient of performance

GSHP ground source heat pump

PSTL proportion of the shifted thermal load (%)

1. Introduction

Geothermal heat, due to its wide availability, has been considered as a renewable and sustainable energy source for building cooling and heating [1, 2]. Shallow geothermal exploitation is even favourable in urban areas, because the accelerated heat fluxes from the warm basement often lead to elevated temperatures in the subsurface [3, 4]. In modern building projects, a common practice is to install dozens of Borehole Heat Exchangers (BHE) prior to the building construction and then connect them through a pipe network to form a BHE array. This array is later connected with heat pumps to extract or inject thermal energy out of or into the shallow subsurface [5, 6]. A recent trend in the industry is to build large BHE arrays with hundreds or sometimes thousands of BHEs to meet the high demand from commercial buildings and residential neighbourhood [7].

Despite of minor differences, most countries follow the same design procedure for large BHE array as the guideline recommended by the American Society of Heating, Refrigerating and Air-Conditioning Engineers (ASHRAE) [8]. It is based on the well known line source method originally developed by Carslaw and Jaeger [9] and later promoted by Ingersoll and Zobel [10]. First, the thermal load of the building is quantified. This load is divided into three successive pulses, i.e. the peak load, the monthly average load, and the annual average load (in kW). When the heating and cooling load is in equilibrium, the total length of all BHEs are then calculated based on the short-term peak load and the effective thermal resistance of the ground. In the second step, the total length is equally divided based on the depth of each BHE, so that the number of BHEs to be installed on site can be determined accordingly. If the heating and cooling load is not balanced, then the penalty temperature T_p and the total BHE length will be calculated in an iterative manner. Based on the ASHRAE procedure, several alternative methods have been developed in recent years, to improve the calculation of T_p in particular [11, 12]. Ahmadfard and Bernier [13] have presented a comprehensive review on the available BHE array designing procedures. In both the original ASHRAE guideline and all the extended procedures, the minimum borehole separation distance S is always defined as an empirical parameter to reduce thermal interference between individual boreholes, and it is also used in the calculation of penalty temperature T_p (cf. Chapter 35.1 in [8]).

When looking into different countries, the regulation on this minimum distance S is not exactly the same. The ASHRAE guideline in United States fix the S value at 6 m [8]. Switzerland requires a minimum distance of 5 m (cf. Miglani et al. [14]). In Germany, this value has been increased from 5 m to 6 m in the 2019 updated VID guideline [15, 16]. In China, a distance between 3 m to 6 m is recommended [17]. In Sweden, a much larger distance of 20 m is enforced (cf. Haehnlein et al. [18]). Due to the fact that different countries have varying climate conditions and initial soil temperatures, this minimum distance S value remains a parameter that is empirically determined. Another issue in the ASHRAE and other guidelines is that the specific heat extraction rate is assumed to distribute equally on each BHE and spread evenly along the entire borehole length. This assumption holds true under the ideal condition where no thermal interference exists among BHEs. However, during the long-term operation, thermal interaction is difficult to avoid and it often varies in space and also over time. Details about this shifted thermal load behaviour could be found in our previous work (Chen et al. [19]) through numerical simulation, or from the work of You et al. [20] through an analytical analysis. Furthermore, if the BHEs are connected in a sequential manner, it is not possible to have identical heat extraction rate on each borehole [21].

In most BHE array projects, the annual cooling and heating load is often not fully balanced. This means thermal plumes can form and accumulate in the subsurface, causing the working fluid temperature to gradually increase or decrease over time. In extreme cases, this may lead to freezing in the vicinity of the BHE or causing the failure of the heat pump [22, 23, 24]. Instead of the adjacent distance S and penalty temperature T_p, the size of a BHE array is more constrained by the outflow temperature of the circulation fluid. In cooling applications, this temperature normally should not exceed 35 °C, otherwise the heat pump will not be working efficiently. When operated in heating mode, the circulation temperature has to be kept above 0 °C [13], in order to mechanically protect the heat pump and avoid ground freezing. As mentioned above, engineers who are designing the BHE array would like to have a calculation procedure, in which the change of circulation fluid temperature can be accurately estimated. In order to do that, a scientific question has to be answered first, i.e. how will the circulation fluid temperature change in response to the imbalanced thermal load, when the thermal interaction in a BHE array can not be avoided?

One obstacle preventing the exploration of the above scientific question is the lack of monitoring data. In order to fully capture the system behaviour, both the annual amount of imbalanced heat imposed on the BHE array and the responding ground loop temperature have to be quantified. This means, sensors and flow meters have to be installed on the inlets and outlets of the building loop, the heat pumps, and also different branches of the ground loops. Continuous monitoring has to be conducted for several years, in order to catch the trend in circulation fluid temperature. Fortunately, Naicker et al. [25] has recently carried out such an intensive monitoring campaign and made the data available to the general public. Their BHE array project is located in Leicester, UK (hereafter as Leicester Project). The building thermal load, heat pump operation, and also ground loop temperatures have been monitored for over 3 years with minute-wise data readings. Detailed introduction of the project is available in Naicker's PhD thesis [26], as well as in his following publications [27, 25]. Interested readers may also access the monitoring data set from the Research Data Archive at the University of Leeds [28].

In this study, we investigate the BHE array behaviour under imbalanced annual thermal load by conducting a series of numerical experiments based on the Leicester project monitoring data. In Sec 2, the mathematical background of the numerical model is introduced. In Sec 3, the numerical model is set up based on the Leicester project and validated against the monitored data set. Analysis on the modelling results reveals the thermal imbalance and thermal interaction among BHEs. In Sec 4, a series of extended numerical experiments are designed and simulated, aiming to investigate the relationship between the circulation fluid temperature change and the amount of imbalanced thermal load. Since the form and accumulation of thermal plume is a critical issue for the long-term operation of a BHE array, the amount of stored thermal energy in the subsurface has been carefully analysed and quantified. Discussions (Sec 5) are also given on the potential implications of our findings.

2. Method

As discussed in our previous work [19], most analytical approaches have difficulties in quantifying the thermal interaction in large BHE arrays. In comparison, numerical models offer more flexibility, by considering different boundary conditions, thermal recharge from the ground surface, groundwater flow and also the geothermal gradient effects [29, 30, 31, 32, 33]. For the large BHE array considered in this work, a pipeline network is always present, coupling the BHEs and the heat pump. The thermal behaviour on each BHE will be affected by this network over the long-term operation. Recently, we have presented the OpenGeoSys (OGS) model that takes the above-mentioned factors into account ([19]). In the HeatTransportBHE module of the OGS software, the variation of BHE outlet temperature and surrounding soil temperature field can be simulated by the dual-continuum approach. In the finite element mesh, the BHE is considered as line elements, while the surrounding soil is represented by prisms. The heat fluxes between BHE wall and the surrounding subsurface are quantified by the coupling term. Readers who are interested in this numerical scheme may refer to Al-Khoury et al. [34] and Diersch et al. [35, 36] for more detailed explanation.

For the coupling of a pipeline network, the open-source simulator Thermal Engineering Systems in Python (TESPy) is introduced. Developed by Witte [37], TESPy is capable of simulating a pipe network with both the thermal and hydraulic balance equations. The nonlinear feature of the coupled equations require the Newton-Raphson iteration, in order to solve for pressure, mass flow and fluid enthalpy at each conjunction point. In OGS, the Python interface library pybind11 is embedded and used for the communication between OGS and TESPy. In this study, the OpenGeoSys version 6.2.2 and the TESPy version 0.2.0 is used accordingly. For more information on the coupling between OGS and TESPy, please refer to Chen et al. [19], and also the online documentation [38], in which detailed tutorials are available to the general public.

3. Modelling Leicester Project

3.1. Project description

In the Leicester Project [25], a large BHE array was installed. It is selected in this work as the reference to validate our numerical model. This system is configured to provide both heating and cooling to the Hugh Aston building with a total floor area of 16,467 m^2. The designed peak cooling capacity of this project is 360 kW through the Fan Coil Unit (FCU) and Air Handling Unit (AHU). The corresponding peak heating capacity is 330 kW through a underfloor heating system. The source side is equipped with 56 borehole heat exchangers, each of which has a depth of 100 m and a diameter of 125 mm. In the basement of the building, there are four water-to-water heat pumps which are all reversible for both cooling and heating application. A single variable speed circulation pump is installed for the ground loop, so that it is able to adjust the flow rate according to the operation condition of the heat pumps. Before construction, a thermal response test (TRT) was carried out on site and the result was evaluated based on the conventional line-source model. The geotechnical characteristics, including initial ground temperature, thermal conductivity and volumetric heat capacity of the subsurface were determined by the TRT. All detailed parameters and array layout could be found in Table 1 and Fig. 1, respectively.

3.2. Model setup

A comprehensive 3D numerical model (Fig. 1(a)), which comprises a BHE array, the surrounding subsurface, and a coupled pipeline network, is established according to the design of Leicester project described above [25]. The model domain is shown in the left part of Fig. 1(a). The subsurface domain around the BHE array has a size of $280 \times 220 \times 151$ m. In it, the soil part is discretized with prism elements, while the BHEs are represented by lines. In total, the mesh contains 69,275 nodes and 130,128 elements. The 56 BHEs are placed in the centre of the domain according to their real-world location. Each BHE has a single U-shape pipe (1U type) installed in it. The BHE top is set at a depth of 1 m from the surface. The arrangement of the array is illustrated in Fig. 1(b), which is in consistence with the original planning. Most of the BHEs have a distance of 5 m to its adjacent ones. However, BHE #11 is only 2 m away from its closest neighbour, exactly following its coordinates reported in Naicker et al. [25].

According to the ground loop configuration, a simplified closed-loop pipeline network is configured in the TESPy software (see the right part of Fig. 1(a)). Pre-defined components in the network are borehole heat exchangers (BHEs), water pump and heat pumps. Since in this study only the working condition on the ground side is investigated, the measured and reported ground loop thermal load in Leicester project is directly imposed as the thermal boundary condition in the BHE array model. The black lines in the network denote to the connection pipes between the components. And the arrows indicates the flow direction of the circulating fluid. After lifted by the water pump, the circulating fluid flows into the array with 56 parallelly connected BHEs. As shown in Fig. 1(b) the entire array is divided into two parts, which is achieved by adding two sub-splitter and merge components in the network (see Fig. 1(a) right). After circulating through each sub-array, the outflows are mixed at the merging point and then flow back to the heat pump, where the heat is either extracted to or injected based on the load profile from the building side. The physical configuration of each BHE pipe in the TESPy network are assigned with the same parameters as those used in the OGS model. They are listed in Table 1 for reference.

Since there is no detailed information for the connection pipes on the ground side from the report of Leicester project, we have configured the model in a way that only the hydraulic and heat loss within the U-pipe in the BHEs are considered, while those loss along the connecting pipes are assumed to be negligible.

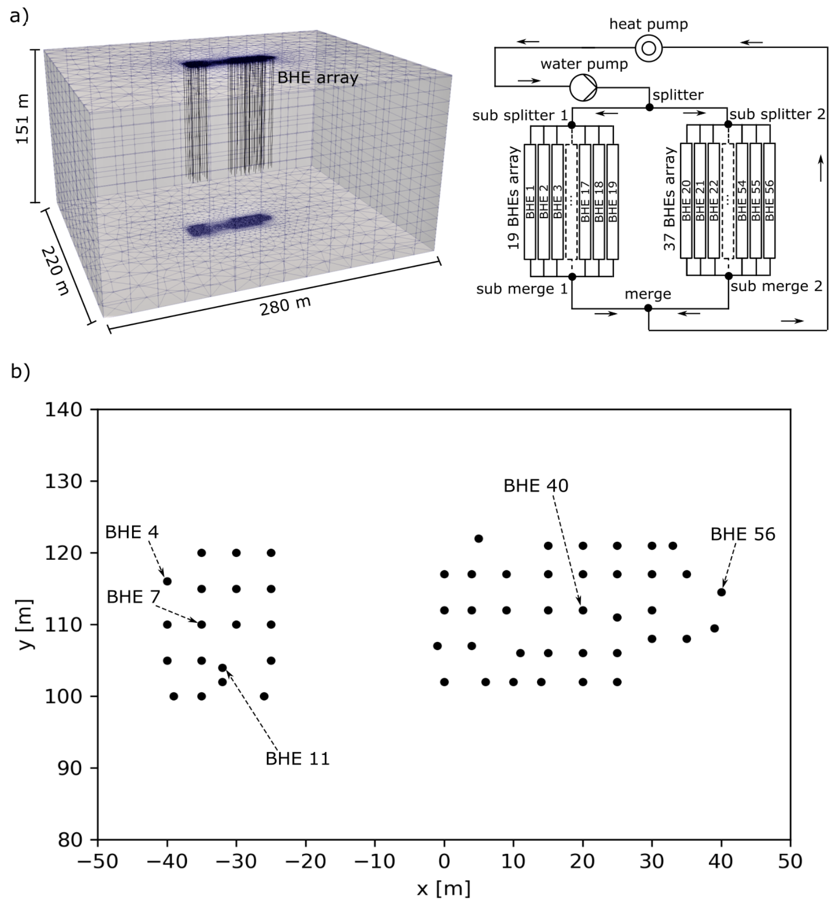

Figure 1: (a) Left: 3D model domain representing the Leicester project in OGS; Right: 56 BHEs pipeline network model; (b) Arrangement of 56 BHE array.

Table 1: Model parameters

Parameter	Symbol	Value	Unit
Initial soil temperature	T_{ini}	11.7	°C
Soil thermal conductivity	λ_s	3.4	$\mathrm{W\,m^{-1}\,K^{-1}}$
Soil heat capacity	$(\rho c)_s$	2576	$\mathrm{kJ\,m^{3}\,K^{-1}}$
Length of the BHE	L	100	m
Diameter of the BHE	D	0.125	m
Pipe inner diameter	d_p	0.026	m
Wall thickness of pipe	b_p	0.003	m
Wall thermal conductivity of pipe	λ_p	0.4	$\mathrm{W\,m^{-1}\,K^{-1}}$
Grout thermal conductivity	λ_g	0.656	$\mathrm{W\,m^{-1}\,K^{-1}}$
Grout heat capacity	$(\rho c)_g$	2700	$\mathrm{kJ\,m^{3}\,K^{-1}}$
Circulating fluid density	ρ_f	1020	$\mathrm{kg\,m^{-3}}$
Circulating fluid heat capacity	$(\rho c)_f$	3962	$\mathrm{kJ\,m^{3}\,K^{-1}}$
Circulating fluid thermal conductivity	λ_f	0.485	$\mathrm{W\,m^{-1}\,K^{-1}}$
Circulating fluid dynamic viscosity	η	0.0024	Pa s
Length of the pipe for BHEs in the network	l	200	m
Diameter of the pipe for BHEs in the network	d_p	0.026	m
Pipe Roughness coefficient for pipes in the network	k_s	0.00001	m

3.3. Initial and boundary conditions

Subsurface Part

Initially, the soil temperature is set to 11.7 °C in the whole model domain. A Dirichlet-type boundary condition is assigned on the surface of the domain with a ground surface temperature curve, which follows the corresponding measured daily mean air temperature in Naicker et al. [25]. The lowest air temperature reaches −5 °C in the winter and the peak temperature in summer is about 24 °C.

BHE Array Part

In TESPy, the Darcy-Weisbach equation (Eq. (1)) is adopted to quantify the hydraulic head loss caused by the friction in the U-pipe within the BHE.

$$\begin{aligned} p_{in} - p_{out} =& \frac{\rho_f}{2} \cdot v^2 \cdot \frac{\zeta\left(\mathrm{Re}, k_s, d_p\right) \cdot l}{d_p}. \\ =& \frac{8 \cdot \dot{m}_{in}^2 \cdot l \cdot \zeta\left(\mathrm{Re}, k_s, d_p\right)}{\rho_f \cdot \pi^2 \cdot {d_p}^5}. \end{aligned} \tag{1}$$

where the calculating flow velocity v is deduced through the pipe's dimensions, the fluid's density and mass flow rate $\dot{m}$ in TESPy. The fluid's density ρ depends on pressure and enthalpy. The Reynolds number Re is a function of pressure, enthalpy and flow rate.

At each time step, the measured inflow temperature and flow rate (Eq. 2) are assigned as the boundary conditions for the simulation in TESPy. In the Leicester project, the measured inflow temperature and flow rate are given by every minute. These measured values can not be directly imposed in the numerical model, as the time step size is fixed to be 1 hour (see our description in the following section). To resolve this discrepancy, minute-wise monitoring data is aggregated. First, those noise readings, the values of which are way beyond a reasonable range, are removed. The date set, containing ca. 1.02 million entries altogether, are aggregated to an averaged value per hour. The average is achieved by calculating the weighted mean of the measured inflow temperature values,

$$T_{aver} = \frac{\sum\limits_{i=1}^{60} T_i \dot{m}_i}{\sum\limits_{i=1}^{60} \dot{m}_i}, \tag{2}$$

where T_i and $\dot{m}_i$ are the measured inflow temperature and flow rate at each measurement interval ($\Delta T = 1\,\mathrm{min}$). At the same time, the average flow rate is calculated by the arithmetic mean of the measured values.

As mentioned in Sec 3.2, since the time step size in this model is set to 1 hour, the model is not capable of predicting short-term behaviour of the BHE array. However, despite of more than 130,128 mesh elements and a total of 17,237 time steps, it is possible to complete the two-year long validation simulation (cf. Sec 3.4) within 129 hours using a small workstation equipped with a 3.40 GHz CPU and 16 GB of memory.

3.4. Model validation

To validate the OGS-TESPy numerical model, the two years long operation phase of BHE array is simulated with the aforementioned configurations. The simulated outflow temperature, as well as the amount of exchanged heat, is compared with the corresponding measurements and presented in Fig 2. The exchanged amount of heat in each month is estimated using the following equation,

$$Q = \int c_f \dot{m}(T_{in} - T_{out})dt, \tag{3}$$

where c_f is the specific heat capacity of the circulating fluid. As mentioned in Sec 3.1, although the measured inflow temperature has been aggregated in order to be used as the model input, the simulation predicted outflow temperature evolution still fits the monitored values very well. As stated in [25], a modest year-by-year increase in the outflow temperature is observed between the first and second year. This phenomena can also be seen in our modelling results. Moreover, both the calculated and measured amount of heat have a consistent tendency in the temporary evolution, which corresponds well to the evolution of the outflow temperature. The slight discrepancies between the measured and computed amount of heat in some months, e.g. in the 15-th, 16-th, 20-th and 21-st month, are most likely caused by the averaging of the measured inflow temperature values. Quantitatively speaking, the accumulated amount of heat injected in the simulation (using the processed data) is about 3.2% higher than in the original data measured data.

3.5. Analysis of the Model Predictions

3.5.1. Subsurface Thermal Imbalance

Through the two-year long operation of Leicester project, the subsurface part was dominated by heat injection process, which can lead to thermal accumulation especially in the centre field of the BHE array. In Fig. 3, the

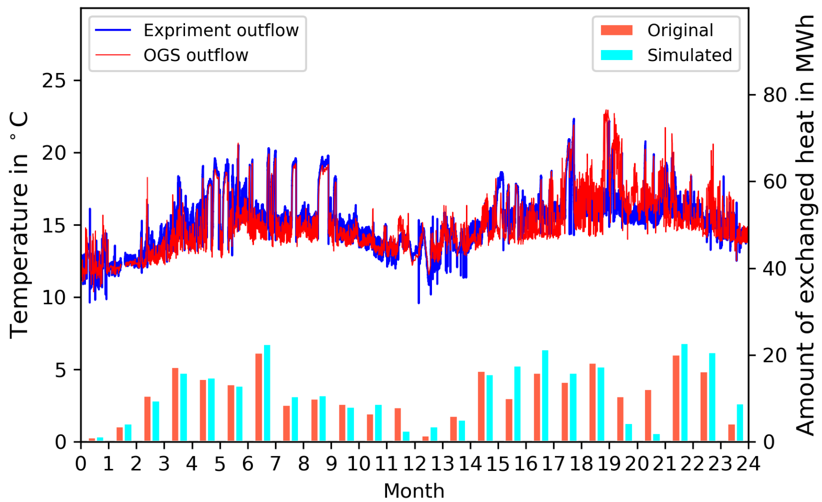

Figure 2: Comparison of the numerical result for the the evolution of the outflow temperature over 2 years with the original data.

computed soil temperature distribution after 2 years of operation is illustrated. Our suspicion is confirmed by the model prediction, as the elevated temperature in the centre area of the array can be clearly recognised. In Fig. 3 lower figure, the maximum temperature increment in the centre is about 2.6 °C. Obviously, the thermal accumulation in the right array is more intensive than that in the left array, as the former part has more BHEs installed than the latter one.

To investigate the temporal evolution of the soil temperature over time, five points (#P4, #P7, #P11, #P40 and #P56) (Fig. 3) are selected. They are located at a depth of $z = -51$ m, and 1 m away from their closest BHEs (BHE #4,#7,#11,#40 and #56 in Fig. 1(b) accordingly).

Fig. 4 illustrates the soil temperature at all five points at the end of each month over 2 years' operation. Compared to the temperature evolution at points #P4 and #P56, the temperature increase at #P7 and #P40 is more intensive. This indicates that the thermal accumulation effects are concentrated in the centre of each array, where #P7 and #P40 are located. After 2 years' operation, a 1 °C temperature difference is predicted between #P4 and #P7 in the left array, while a greater difference of 1.3 °C is found between #P40 and #P56 in the right array. Meanwhile, #P40, which is

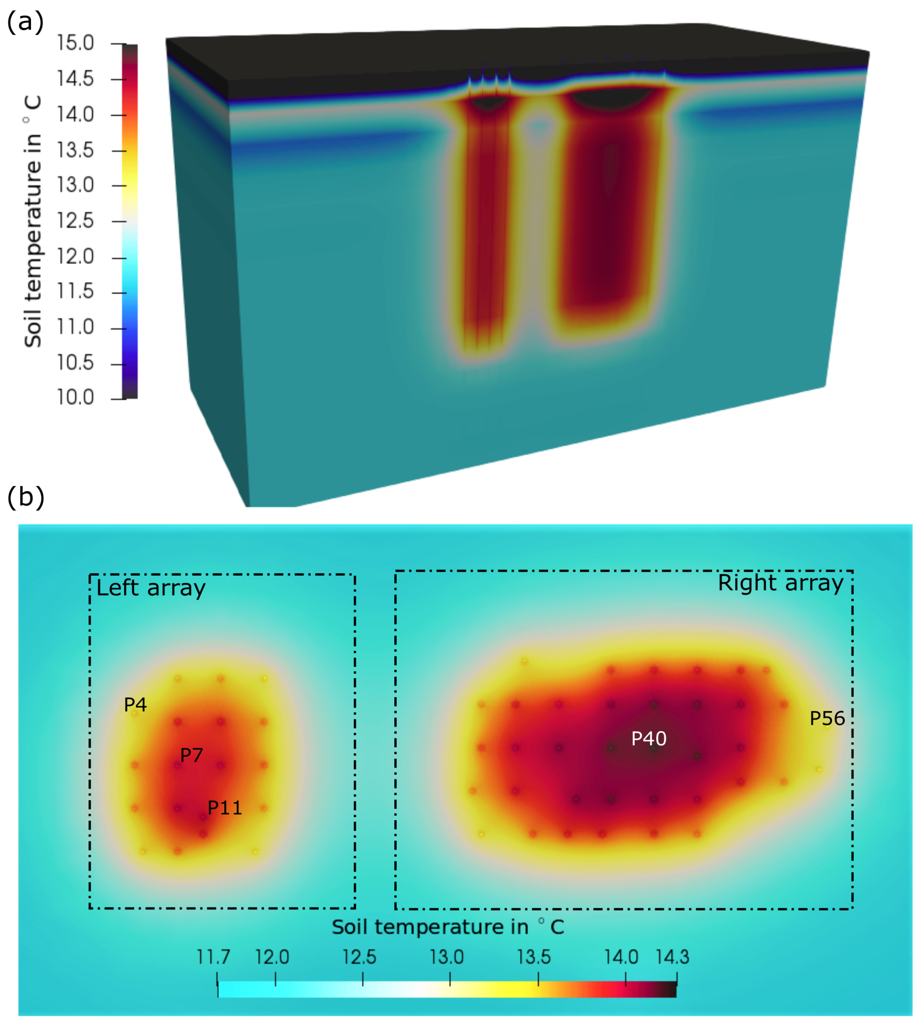

Figure 3: (a): Vertical cross-section of the 3D soil temperature distribution in the middle of the array after 2 years; (b): Horizontal view of temperature distribution at a depth of $-51\,\mathrm{m}$.

located in the centre of the right sub-array, is predicted to have a slightly higher temperature of 0.3 °C than that at #P7, which locates in the left sub-array. This strong variation at #P40 could have resulted from the influences of BHEs from both sub-arrays sides. It can be seen from the upper part of Fig. 3 that thermal accumulation does happen between the left and right arrays. Overall, the modelling result indicates that the array with more BHEs could produce more intensive imbalance in the underground. Among the five points, the strongest temperature variation is found at #P11. It increases more intensively during the first 6 months since it is affected by two nearby BHEs at the same time. To sum up, the soil temperature is not solely affected by the nearby BHEs. Further, the accumulative thermal process in a BHE array could have strong influence on the temperature distribution as well in the long term.

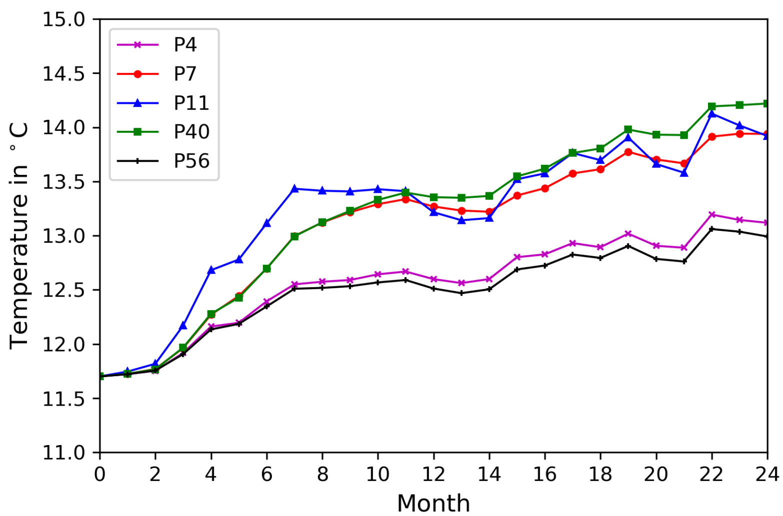

Figure 4: Evolution of the soil temperature on the selected points in the end of each month over 2 years.

3.5.2. Load shifting behaviour

As stated in our previous work (Chen et al. [19]), the interactions among the BHEs during long-term system operation can lead to load shifting in the BHE field. The monitoring data obtained from Leicester project provides an excellent opportunity for us to further investigate the trend of load shifting under realistic conditions. The heat injection rate at four represent BHEs, i.e. BHE #4, #7, #40 and #56 is quantified based on the simulated inflow and outflow temperature on each BHE. In Fig. 5, the percentage of the shifted thermal injection rate (hereafter as PSTL) on BHE is calculated by

$$\mathrm{PSTL_i} = \frac{\dot{Q}_i - \dot{Q}_{mean}}{\dot{Q}_{mean}} \times 100, \tag{4}$$

where i refers to the index of the BHE. $\dot{Q}_i$ and $\dot{Q}_{mean}$ are the heat injection rate at i-th BHE and the mean heat injection rate, respectively.

In Fig. 5(a), a general trend can be observed that the thermal load is gradually shifted away from the centre to the outer edge of the array. The heat injection rates on the centre BHEs (#7 and #40) are lower than the designed average value (PSTL < 0), while they become higher than the mean value (PSTL > 0) at the edge BHEs (#4 and #56). The reason behind is that the soil temperature in the centre part is generally higher than that in the outer area (cf. Fig. 3). Moreover, the thermal shifting is found to be stronger in the right sub-array (BHE #56 and #40) than in the left part, as more BHEs are installed in the right area. In Fig. 2(a), the most intensive shifting (PSTL value of 60.7%) is found in the 12-th month of the first year, where the system has the lowest thermal demand. This phenomena is consistent with the observations reported in our previous work [19].

In Fig. 5(b), the load shifting phenomenon between the left and right sub-array is further investigated. If there is no thermal interaction, each BHE should deliver same amount of heat, as they are connected in a parallel manner. Following this assumption, the rate of extracted heat from the left or right sub-array should be according to the corresponding number of installed BHEs, i.e. following a ratio of 19 : 37. Using this proportion as a reference, the amount of shifted heat ΔQ of the left or right sub-array can be quantified by first integrating the amount of extracted heat on each BHE, and then comparing it with the reference value. In Fig. 5(b), the monthly change of ΔQ and its corresponding percentage of deviation PSTL is depicted for each sub-array. It can be found that, after 4 months of heat injection, the heat extraction rate shifts gradually from the right towards the left array. The reason behind is the soil temperature difference in the left and right part during the system operation. As shown in Fig. 3(b), a higher soil temperature can be found in the right array after 2 years. This is mainly caused by the more number of BHEs on the right side. As the inflow temperature is kept consistent by the pipe network for all BHEs, the actual heat injection rate on each BHE is dependent on the temperature difference in comparison to the surrounding soil. By comparing the actual simulated value with the design reference, the shifting phenomenon is well observable. With regard to the shifted percentage, the maximum value is found to be about 8.6% in the left sub-array and it is observed in the 12-th month. This is in good agreement with the result shown in the Fig. 5(a). The amount of heat shifted away from the right array is fully transferred to the left part. Therefore, due to the fact the original designed load on the left is only about half (19 : 37) of that on the right, the percentage of elevated extraction rates on the left is about twice as much as that on the right side.

Fig. 5(c) shows the performance of two BHEs, i.e. BHE #40 and #56 at two selected moments. At time $t1 = 17,007$ hour, the system is dominated by heat injection, while at $t2 = 17,011$ hour heat extraction is the main process. BHE #40 is located at the centre of the right sub-array, while BHE #56 is at the edge. At $t1$, the heat injection rate of BHE #40 drops by about 39%, while it increases by about 43% on BHE #56. In the heat extraction dominated period ($t2$), the corresponding values at BHE #40 and #56 are switched to +56% and -62%, respectively. It indicates that in the long-term operation of a BHE array, when both heating and cooling are applied, the thermal recharge of the subsurface can partially mitigate the shifting phenomenon.

4. Extended numerical experiment

4.1. Scenarios description

In the Leicester project reported by Naicker and Rees [25], the cooling-dominant system was designed with a 360 kW peak capacity. However, if one looks into the monitored data, it can be found that the maximum heat injection rate imposed on the BHE array was only 73 kW, which accounts for only 20.3% of the peak designed capacity. Considering the energy consumption on the heat pump, this rate could be much lower with respect to the actual thermal load at the ground side during the system peak cooling capacity. Since there is no reported information for both the actual COP curve and the peak cooling capacity of the BHE array in the project, we assumed the (360 kW) peak cooling capacity of building as the peak cooling load on the BHE array at the ground side. Therefore, it is interesting to see the long-term behaviour of the system, if the actual heat injection rate is gradually approaching the designed peak. In this context, five additional scenarios (numbered from #1 to #5) are numerically simulated with gradually increasing heat injection rates. We choose to lift the total amount

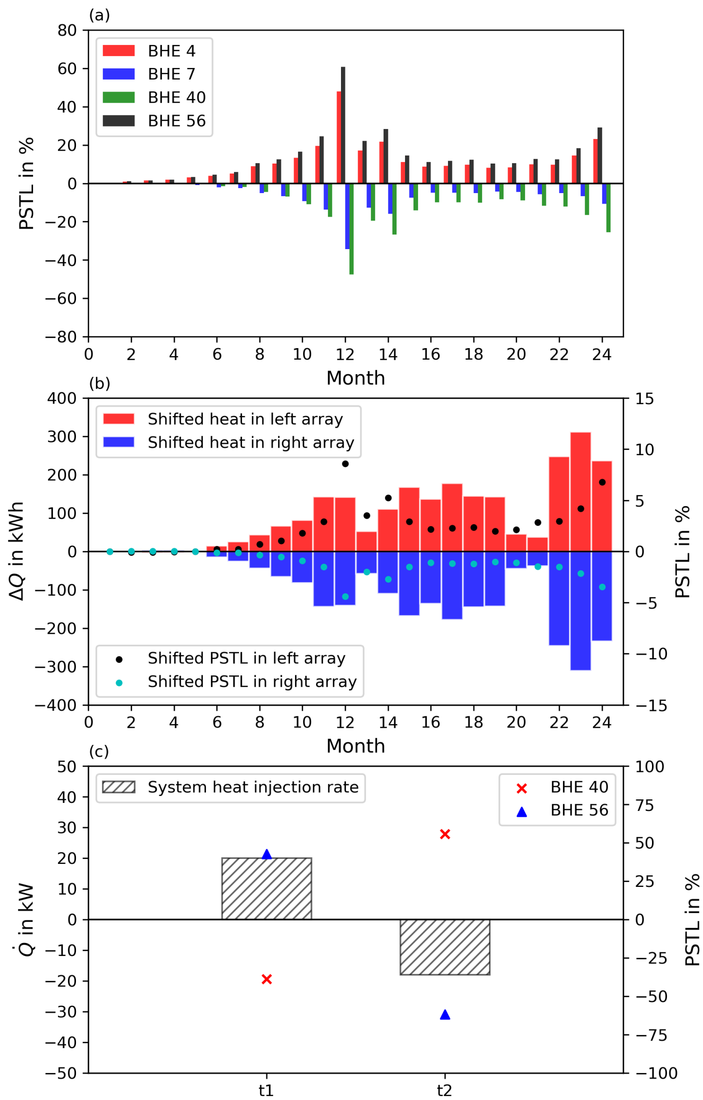

Figure 5: (a) Monthly averaged percentage of shifted thermal injection rate on the selected BHEs over the 2-year period; (b) Monthly total amount of shifted heat and the corresponding averaged percentage values in the left and right sub-array; (c) Percentage of shifted thermal injection rate on the selected BHEs at time $t1 = 17,007$ hour and $t2 = 17,011$ hour.

of exchanged heat imposed on the array to 100%, 197%, 296%, 395% and 493% of the real observed value in the first year operation of the Leicester project. Under these conditions, the original designed peak capacity could be reached, while the characteristics of the load profile remains unchanged. From the second year forward, the annual system thermal load profile is specified to follow that of the first year and repeats itself until the end of 20-th year. All five scenarios are then simulated to reveal the long-term behaviour of the BHE array.

Since the simulation aims to investigate the long-term behaviour and does not focus on its short-term responses, a monthly averaged system thermal load is specified in each scenario. The original measured values are reported in every minute, thus a conversion calculation is performed. By executing two steps, the resulting load profile specified in scenario #1 (The red line in Fig. 6(b)) is generated. The minute-wise extracted (heating mode, in negative MWh values) or injected (cooling mode, in positive MWh) heat is integrated separately over each month using the equation (Eq. (3)). Summing the absolute values of heat exchanged in these two modes into the total amount of heat exchanged ($Q_{exchanged} = Q_{cooling} + \mid Q_{heating} \mid$) in each month. Subsequently the monthly averaged system thermal load $\dot{Q}_{average}$ is obtained dividing by the duration of the month t_m (Eq. (5)). The positive and negative of this averaged value are then defined as the cooling and heating loads in that month, respectively. The duration of the cooling or heating period in each month could be calculated using equation (6), where $Q_{cooling}$, $Q_{heating}$, and $Q_{exchanged}$ are the amount of the injected heat, extracted heat and total exchanged heat of the system in one month, respectively.

$$\dot{Q}_{average} = \frac{Q_{exchanged}}{t_m} \tag{5}$$

$$t_{cooling/heating} = \frac{\mid Q_{cooling/heating} \mid}{Q_{exchanged}} \cdot t_m, \tag{6}$$

According to Ahmadfard and Bernier [13], the monthly total flow rate could be set to $0.25\,\mathrm{L\,s^{-1}}$ per kW of the thermal load (Fig. 6(b)). By observing the data reported by Naicker et al. [25], the minimal and maximal flow rates of the system were between $2\,\mathrm{L\,s^{-1}}$ and $30\,\mathrm{L\,s^{-1}}$, respectively. In our numerical model, the circulation flow rate is then set to be linearly dependent on the absolute value of system thermal load, while being kept within the same minimum and maximum range. On the upper boundary of the model domain, an averaged monthly air temperature curve is imposed as Dirichlet boundary condition, based on the data reported in the first year operation [25] (cf. Fig. 6(a), black line). Following the designed logic described above, the annual system thermal load and flow rate in scenario #2 to #5 are adjusted proportionally, i.e. 197%, 296%, 395%, 493% based on scenario #1. As a consequence, the monthly exchanged heat in each scenario is also lifted proportionally, as illustrated in Fig. 6(a). In scenario #5, the peak system thermal load is set to be 173.6 kW, which is still only ca. half of the original design. All other settings of scenario #2 to #5 remain the same as those presented in Sec 3.

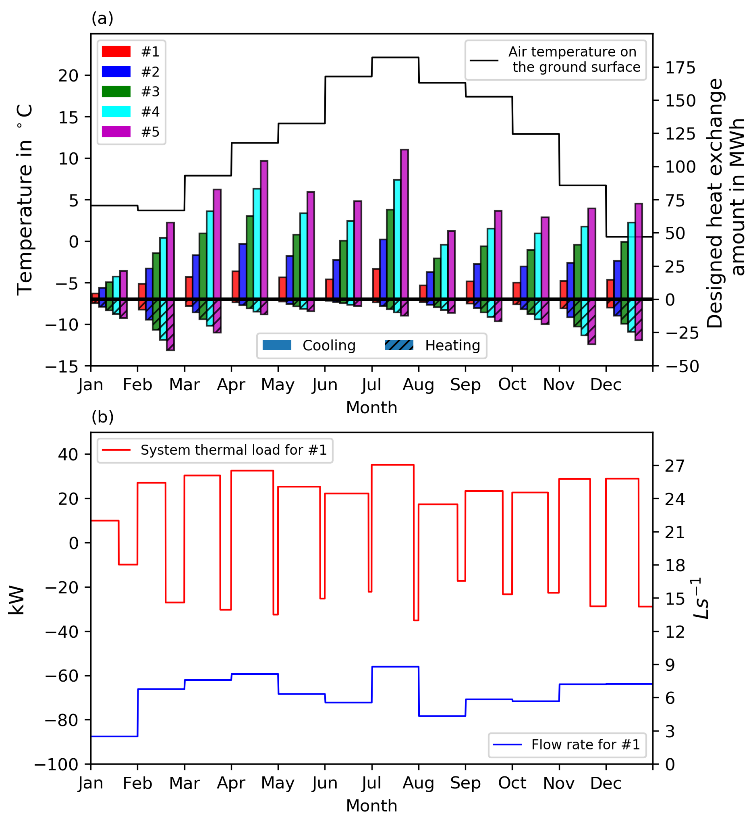

Figure 6: (a) Designed monthly heat exchange amount in the 5 scenarios and the annual air temperature on the ground surface. (b) Profile curve of system thermal load and flow rate specified in scenario #1.

4.2. Results and analysis

Fig. 7(a) illustrates the simulated temporal evolution of the outflow temperature in all five scenarios. To ensure a sustainable performance of the BHE array, the temperature of circulation fluid at the inlet of the heat pump should usually be kept below 35 °C in the cooling mode [13]. This 35 °C threshold is indicated with a dotted line in this figure. Since the system is dominated by heat injection, a gradual but steady increasing trend in the outflow temperature is observed in all five scenarios, although with different magnitudes. Among the five scenarios, the lowest temperature of 16.3 °C is observed after 20 years in scenario #1, where the amount of exchanged heat is minimum. The most intensive increase happens in scenario #5, where the thermal load is the highest. After 20 years' operation, the highest outflow temperature in scenario #5 reached 34.5 °C, which is already approaching the 35 °C threshold. This suggests that the BHE array can be sustainably utilised for 20 years, but not much longer, if the actual imposed thermal load is close to the designed maximum heat capacity as reported in [25]. However, in our model the peak cooling load at the ground site is assumed to be identical as the reported designed peak load from the building side. When considering the energy consumption on the heat pump, a higher peak cooling load at the ground site could be expected. Therefore under real working condition, the designed peak cooling load at building site may cause an elevated outflow temperature from the BHE array to exceed 35 °C.

In Fig. 7(a), with the alternating cooling and heating load imposed, the outflow temperature shows a monthly fluctuation pattern. In scenario #1, with the lowest heat extraction rate ($6.3\,\mathrm{W\,m^{-1}}$ on each BHE), the temperature fluctuation is found to be the weakest with a magnitude of about 1.5 °C. The strongest fluctuation is observed in scenario #5, with the highest heat exchange rate in all 5 scenarios ($31\,\mathrm{W\,m^{-1}}$). The deviation between the annual highest and lowest outflow temperature accounts for 11.5 °C. As aforementioned, the imposed system thermal load is averaged on a monthly basis, hence a much stronger fluctuation in the fluid temperature could be expected in real operations, especially when a high peak cooling load is imposed.

The maximum rise in outflow temperature from all five scenarios are evaluated and presented in Fig. 7(b). Assuming the subsurface is thermally not disturbed, i.e. there is no additional heat injected or extracted, then the outflow temperature from the BHE array should equal to the initial soil temperature. This reflects the physical meaning of the origin point in Fig. 7(b). From scenario #1 to #5, the amount of additional heat is gradually increased. As a result, the increment in outflow temperature is also rising accordingly. In Fig. 7(b), both the maximum and mean outflow temperature rise in each scenario are plotted against the total amount of accumulated heat at the end of 20-th year. It is interesting to find that, the rise in both maximum (red dots) and mean (blue crosses) temperature increments follow strict linear relationships with the amount of accumulated heat injected into the subsurface through the BHE array. Meanwhile, it is also noticed that the two slopes are distinctly different. This suggest that even with the same amount of accumulated heat, the outflow temperature can also be fluctuating due to the peak load imposed on the array. Based on the simulated data, the correlation between ΔT and ΣQ can be fitted perfectly with two linear regression lines with R-squared values of 99.989% (maximum ΔT) and 99.982% (mean ΔT). Both temperature trends hint us that when other factors, such as the distance between the boreholes and the soil heat capacity is considered, it is possible to develop a simplified formula to estimate the change of system outflow temperature in response to the total amount of imbalanced heat accumulated over the years. Moreover, once the linear relationship is identified, the acceptable amount of accumulative imbalanced heat for a particular BHE array can be inversely estimated by giving a threshold value of the working fluid temperature.

4.3. Temporal change of stored heat

In the previous part, it is clearly demonstrated that the elevated soil and circulation fluid temperature, caused by the annually imbalanced thermal load, are the controlling factors whether a BHE array can be sustainably operated in the long-term. Since the elevated soil temperature reflects the amount of heat accumulated in the subsurface, it is important to know how much heat is stored in the subsurface, and also its percentage in comparison to the amount of heat transferred to the building. The amount of stored heat in the subsurface can be quantified by integrating the amount of sensible heat in each element of the soil compartment in one time step, and then comparing that total value with the one at the beginning of the simulation.

Fig. 8(a) illustrates the evolution of the annual amount of stored heat in scenario #3 and its percentage with respect to the total amount of system imbalanced heat. The stored heat increases gradually over the years, from 360 MWh in the first year up to 5043 MWh in the 20-th year. Meanwhile, its percentage drops from nearly 100% at the beginning and stabilises at ca. 70% in the end. This suggests that there is an increasing proportion of imbalanced heat dissipating to the atmosphere through the ground surface. This trend is consistent as the behaviour found in our previous work [30, 19], where a heating-only scenario was analysed. There the thermal

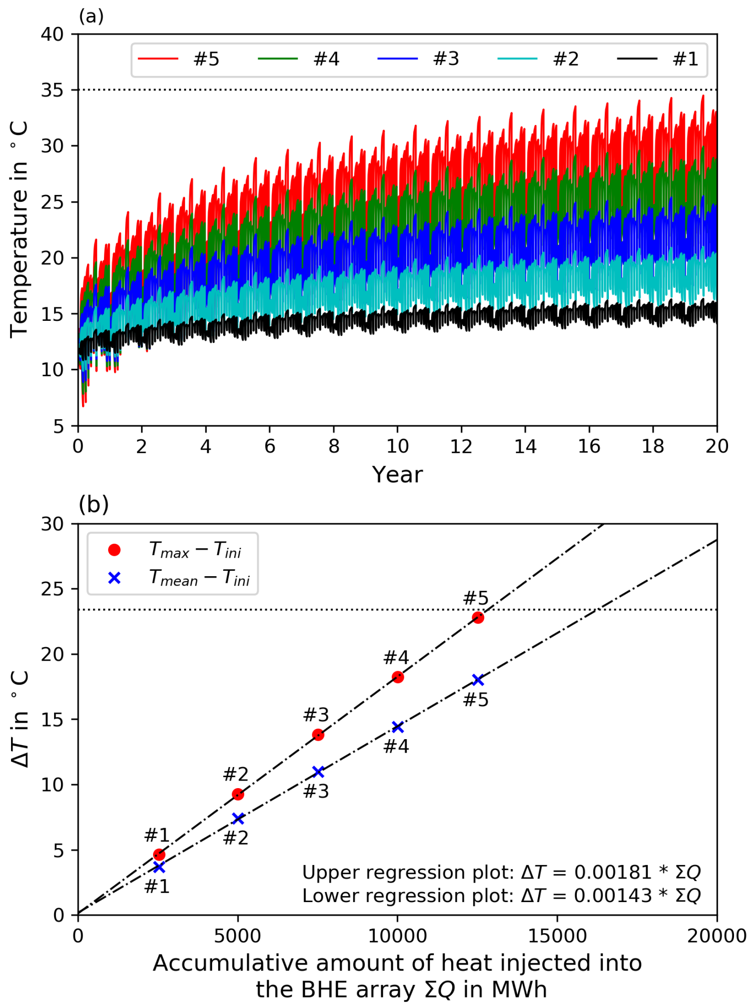

Figure 7: (a) Temperature evolution of the working fluid flowing out from the BHE array in the 5 scenarios over 20 years; (b) Regression plot for the correlation between the maximum and mean outflow temperature against the total amount of accumulated heat injected into the BHE array at the end of the 20-th year.

recharge through the ground surface has a cumulative influence on the soil temperature distribution in and around the BHE array. More specifically, the area with elevated soil temperature will extend itself over the long-term heat injection, thus enhancing the thermal gradient from the subsurface towards the ground surface. Therefore, the amount and proportion of thermal discharge are also elevated over time. Despite of the elevated thermal discharge, analysis on the scenario #3 result reveals that there is still 67.2% of the total imbalanced heat stored in the subsurface after 20 years. When the amount of imbalanced heat increases from 2534 MWh to 12 512 MWh from scenario #1 to #5, the amount of stored heat is also increasing accordingly (see the blue bars in Fig. 8(b)). However, due to the elevated thermal discharge mentioned above, its percentage slightly drops from 70.8% down to 65.6%. Based on the above analysis, one can conclude that over the long-term operation of a BHE array, the majority of the annual imbalanced heat will be stored in the subsurface, and its percentage is less dependent on the amount of heat injected.

4.4. Spatial distribution of stored heat

To further investigate the spatial distribution of the stored heat in the subsurface, we have created two controlled spaces. Each contains a BHE sub-array inside. The boundary of the space is drawn with a 2.5 m distance from the BHE located at the peripheries of the array (see that dark grey area marked in Fig 9(a)). This setup results in a space of 50 000 m^3 for the left sub-array and 158 000 m^3 for the right part. With both parts considered together, the specific stored heat ($kWh\,m^{-3}$) is quantified by normalising the total amount of stored heat over the volume. These specific heat values for 5 different scenarios are depicted in Fig 9(b). These values have been also compared against the total amount of imbalance heat, and the resulting percentages are presented in the same figure.

In the five scenarios, the specific stored heat values increase along with the elevated amount of imbalance heat. In scenario #5, a maximal specific stored heat of 20.0 $kWh\,m^{-3}$ is achieved. According to the findings in Sec 4.2, the temperature of the outflow fluid is already approaching the 35 °C threshold in this case. One can concluded that with the current system design, 20.0 $kWh\,m^{-3}$ can be considered as the upper-limit in the capacity of storing imbalanced heat in the subsurface. When normalising this value by the total amount of imbalanced heat, its ratio remains at around 25%. Combined with the analysis in the previous section, it can be concluded that heat actually dissipates far way from the array location and the thermal plume spreads into a much larger area. For all the heat stored in the

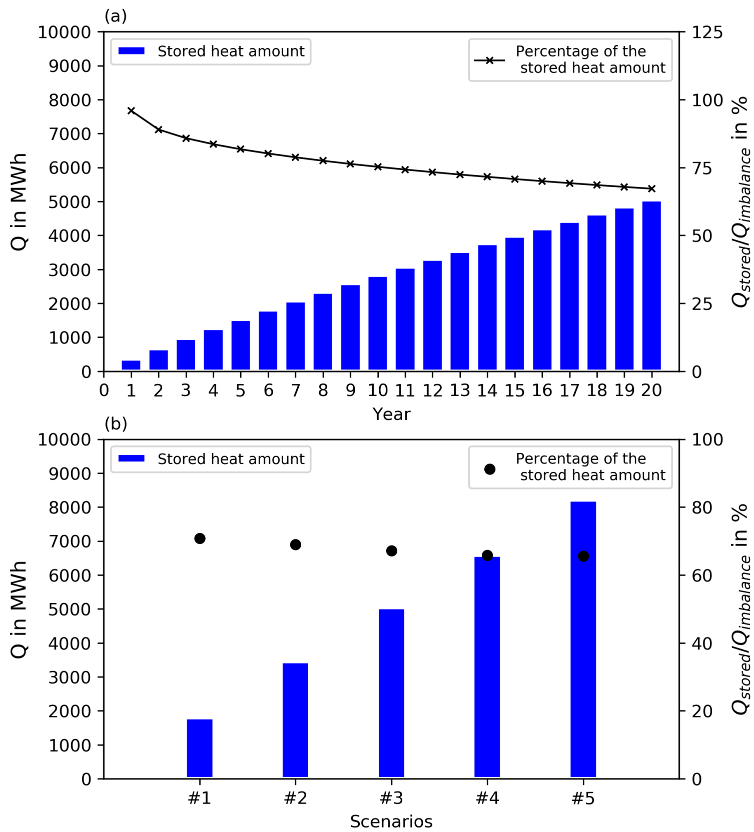

Figure 8: (a) Evolution of the amount of stored heat in the entire domain over 20 years, based on simulated result of scenario #3; (b) Total amount of stored heat and their proportion from scenarios #1 to #5.

subsurface, around 37% is stored in the array area, while the rest goes to the surrounding subsurface.

Nevertheless, if the distance among adjacent BHEs is enlarged, the above specific heat values and ratios may change as well. Here, a preliminary relationship can be illustrated between the amount of stored heat and the respective adjacent distance S. In scenario #5, a 7 m instead of 5 m BHE distance is specified. After 20 years operation, a maximum outflow temperature of 30.5 °C is being predicted, which is lower than the 34.5 °C value when the model is specified with 5 m distance. The reason behind this is the decreasing of the specific stored heat value in the BHE array. As shown in Fig. 9(c), the value decreases from $20.0\,\mathrm{kWh\,m^{-3}}$ to $12.9\,\mathrm{kWh\,m^{-3}}$ when S is enlarged to 7 m. Meanwhile, 32.2% of system total amount of imbalance heat is stored in the enlarged BHE array, which is higher than the 25% value calculated in the 5 m model. Therefore one can conclude that the adjacent distance has an important role in determining the long-term operation behaviour of a large BHE array. To be specific, the adjacent distance is as important as the length of BHE. Thus, the subsurface volume around the BHE array, which is determined by the adjacent distance as well as the length of the BHE, should be considered as one of the characteristic factors in the designing of the BHE array.

5. Discussions

5.1. Pipeline network design

As shown in Sec 3.2, a simplified pipeline network model is built according to the ground loop design reported in the Leicester project. By adopting this coupled feature, the hydraulic states within the entire ground loop could be captured. In all scenarios stated in Sec 4, the average hydraulic loss in the entire BHE array is below 1% compared to the amount of the system thermal load over the long-term operation. A transient maximum percentage with 2.2% can be found in scenario #5, due to the high flow rate there. It should be noticed that all the connection pipes in the circulation loop are assumed to have no hydraulic loss in this study. When detailed information on the material and diameter of the pipes are available, it is more reasonable to consider the hydraulic losses when predicting the long-term behaviour of a large BHE array. In reality, both the form of BHE array and the system operation strategy varies greatly from each GSHP project [39, 21]. Regarding this point, the present numerical model shows its advantage, because it is capable to consider pipeline network with arbitrary connections. In the TESPy network, the hydraulic states for each

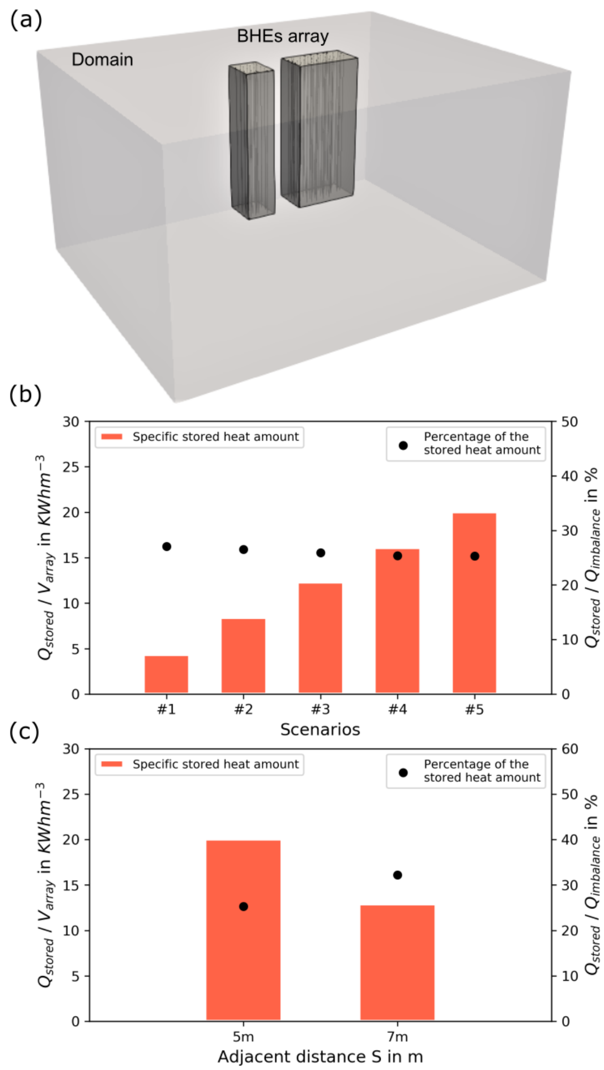

Figure 9: (a) Selected subsurface volume (marked with dark grey); (b) Specific heat stored in the selected volume and its percentage of over the amount of total imbalanced heat after 20 years' operation in the 5 scenarios; (c) Specific heat stored in the selected volume and its percentage of over the amount of total imbalanced heat after 20 years' operation in scenario #5, in models specified with a 5 m and 7 m adjacent distance.

pipe is automatically computed based on the mass and energy conservation. In addition, a temperature dependent heat pump COP curve can also be specified in TESPy as one of the input parameters. With such information at hand, a multiple BHE array system based on the amount of energy consumption at building site can be predicted by our model in a more accurate manner.

Besides, it should be noticed that the heat extraction rate shifting phenomenon shown in Fig. 5 is the effect of current pipe network design. With the parallel BHE array setup, all BHEs are receiving an identical inflow temperature and then deliver different thermal load performances due to the soil temperature imbalance in the array. It indicates that the pipe network itself has an intrinsic feature of re-balancing the thermal load among different BHEs. Therefore it is necessary to simulate a large BHE array system, with the coupled pipeline network explicitly considered. Only in this way, the system behaviour over the long-term operation can be correctly revealed.

5.2. Optimisation of the system operation

As shown in Fig. 5 and discussed in Sec 3.5.2, thermal shifting phenomenon in a large BHE array system can be clearly observed over the long-term operation. When the shifting happens, BHEs located at the edge of each sub-array have larger heat injection rates than the mean designed value, while those BHEs at the centre have lower rate. It should be noticed that such seasonal shifting behaviour is not unique and has already been reported by several researchers. For example, our previous research [19] has investigated the shifting behaviour in detail. This phenomena has also been confirmed in the study conducted by You et al. [20] through an analytical approach. Bayer et al. [40] observed similar pattern and developed an optimisation strategy based on it. They suggested that a given number of BHEs located at the centre of the array should be disconnected from the pipe network in order to mitigate the thermal anomalies in the BHE array subsurface.

Besides, as stated in Sec 3.5.2, when a heating phase is applied in between the cooling seasons, the thermal recharge of the subsurface can partially mitigate the shifting phenomenon. Based on our analysis in the previous section, the heat dissipation pattern can be further utilised to improve the array operation. More specifically, during the heating phase, only those BHEs located at the array centre should be applied, because the elevated soil temperature there allows them to deliver a higher specific heat extraction rate. Also, the cold plume created by heating application can be utilised later on by the BHEs at the peripheries. Such optimisation strategy requires a series of numerical simulations and is currently being investigated by our team.

5.3. Unconsidered factors

As this study is based on the monitoring data from the Leicester project, the amount of heat injected into the subsurface is more than that extracted. Most findings in this work should be considered as only effective for cooling application dominated BHE arrays. However, in heating dominated systems, a similar but inverse trend can be expected. A similar correlation between the drop in fluid temperature and the accumulative amount of extracted heat can also be expected over the long term operation. There, the limiting factor could be the 0 °C temperature limit on the outflow circulation fluid, which is imposed by the heat pump [13]. By considering this limit, the acceptable total amount of extracted heat from the BHE array subsurface for a sustainable system operation can also be estimated.

It is well known that groundwater flow could enhance the capacity of a BHE array, by bringing in additional thermal recharge from the upstream subsurface. In this work, information on groundwater flow is not reported by Naicker et al. [25]. Although the OpenGeoSys code used here is capable of simulating the BHE array under groundwater flow conditions (see e.g. Meng et al. [41]), we assume that there is no groundwater present in the Leicester site. For the majority of shallow geothermal GSHP projects, our assumption is also conservative but safe. Therefore, the main findings and conclusions achieved in this work are applicable to most BHE array projects.

6. Conclusion and outlook

In this work, the long-term behaviour of a large BHE array located in Leicester, UK is investigated by conducting numerical simulations. The model is validated against monitoring data through two years of operation under real working conditions. It is found that heat starts to accumulate in the centre of the BHE array due to higher amount of cooling load imposed on the system. This results in the heat injection rate being gradually shifted from the BHEs in the centre towards those at the edges. At the mean time, the thermal load is also slowly transferred from the right-side array towards the left side.

In the Leicester project, the actual heat injection rate is only 20.3% of its peak designed value. Scenario simulation with gradually increasing heat injection rates reveals that the BHE array can be sustainably utilised for 20 years even under the designed peak thermal load, but likely not any longer.

It is more interesting to find that the rise in outflow temperature follows a perfect linear dependency on the amount of accumulated heat injected into the BHE array. Moreover, it is found that around 37% of the total imbalance heat can be stored in the subsurface volume around the BHE arrays. When the circulation fluid temperature is approaching the 35 °C upper limit, a maximum of 20.0 kWh m^{-3} specific heat can be stored in the subsurface. Nevertheless, when the distance among the adjacent BHEs increases from 5 m to 7 m, the corresponding outflow temperature decreases from 34.5 °C to 30.5 °C, and the specific heat value also decreases to 12.9 kWh m^{-3}. It indicates that the adjacent distance among BHEs has an important role to determine how much imbalanced heat a multiple BHE array can sustain.

As discussed in section 5.2, based on the prediction of seasonal thermal shifting, the operation strategies could be optimised to achieve a higher specific heat extraction rate. More importantly, with the consideration of other factors such as the distance between the boreholes and the soil heat capacity, it is possible to develop a simplified formula to estimate the change of system outflow temperature in response to the total amount of imbalanced heat accumulated over the years. This relationship can help to prevent the system from being overloaded in the long-term operation. However, the exact relationship between the amount of imbalanced heat, the distance between adjacent BHEs, and the increment in circulation fluid temperature, needs to be further investigated in the future.

Acknowledgements

The research work is part of the new Helmholtz Research Program "Changing Earth–Sustaining our Future" Topic 8 "Geo-resources for the Energy Transition and a High-Tech Society" within the program-oriented research (POF IV). This study receives partial funding from the "ANGUS II" project (Grant No 03ET6122B) and the "EASyQuart" project (Grant No 03EGB0016C), which are provided by the German Federal Ministry of Economic Affairs and Energy (BMWi). Both funding is gratefully acknowledged.

References

[1] P. Bayer, G. Attard, P. Blum, K. Menberg, The geothermal potential of cities, Renewable and Sustainable Energy Reviews 106 (2019) 17–30. doi:10.1016/j.rser.2019.02.019.

[2] B. van der Zwaan, F. Dalla Longa, Integrated assessment projections for global geothermal energy use, Geothermics 82 (2019) 203–211. doi:10.1016/j.geothermics.2019.06.008.

[3] K. Zhu, P. Blum, G. Ferguson, K.-d. Balke, P. Bayer, The geothermal potential of urban heat islands, Environmental Research Letters 5 (2010) 6pp. doi:10.1088/1748-9326/5/4/044002.

[4] J. A. Rivera, P. Blum, P. Bayer, Increased ground temperatures in urban areas: Estimation of the technical geothermal potential, Renewable Energy 103(C) (2016) 388–400. doi:10.1016/j.renene.2016.11.005.

[5] U. Lucia, M. Simonetti, G. Chiesa, G. Grisolia, Ground-source pump system for heating and cooling: Review and thermodynamic approach, Renewable and Sustainable Energy Reviews 70 (2017) 867–874. doi:10.1016/j.rser.2016.11.268.

[6] W. Cai, F. Wang, J. Liu, Z. Wang, Z. Ma, Experimental and numerical investigation of heat transfer performance and sustainability of deep borehole heat exchangers coupled with ground source heat pump systems, Applied Thermal Engineering (2018). doi:10.1016/j.applthermaleng.2018.12.094.

[7] T. Kurevija, D. Vulin, V. Krapec, Effect of borehole array geometry and thermal interferences on geothermal heat pump system, Energy Conversion and Management 60 (2012) 134–142. doi:10.1016/j.enconman.2012.02.012.

[8] ASHRAE, 2019 ASHRAE Handbook - Heating, Ventilating, and Air-Conditioning Applications (SI Edition), American Society of Heating, Refrigerating and Air-Conditioning Engineers, Atlanta, GA, 2019.

[9] H. Carslaw, J. Jaeger, Heat conduction in solids, Claremore Press, Oxford, 1947.

[10] L. Ingersoll, A. Zobel, Heat conduction with engineering and geological application, 2nd ed., McGraw-Hill, New York, 1954.

[11] M. Fossa, The temperature penalty approach to the design of borehole heat exchangers for heat pump applications, Energy and Buildings 43 (2011) 1473–1479. doi:10.1016/j.enbuild.2011.02.020.

[12] A. Capozza, M. De Carli, A. Zarrella, Design of borehole heat exchangers for ground-source heat pumps: A literature review, methodology comparison and analysis on the penalty temperature, Energy and Buildings 55 (2012) 369–379. doi:10.1016/j.enbuild.2012.08.041.

[13] M. Ahmadfard, M. Bernier, A review of vertical ground heat exchanger sizing tools including an inter-model comparison, Renewable and Sustainable Energy Reviews 110 (2019) 247–265. doi:10.1016/j.rser.2019.04.045.

[14] S. Miglani, K. Orehounig, J. Carmeliet, A methodology to calculate long-term shallow geothermal energy potential for an urban neighbourhood, Energy & Buildings 159 (2017) 462–473. doi:10.1016/j.enbuild.2017.10.100.

[15] The Association of German Engineers (Verein Deutscher Ingenieure), Thermische Nutzung des Untergrunds Erdgekoppelte Wärmepumpenanlagen; VDI 4640, Blatt 2, Beuth Verlag GmbH, Berlin, 2001.

[16] The Association of German Engineers(Verein Deutscher Ingenieure), Thermal use of the underground - Ground source heat pump systems; VDI 4640, Part 2, Beuth Verlag GmbH, Berlin, 2019.

[17] GB50366, Technical code for ground-source heat pump system, Ministry of Housing and Urban-Rural Development, PR China, 2009.

[18] S. Haehnlein, P. Bayer, P. Blum, International legal status of the use of shallow geothermal energy, Renewable and Sustainable Energy Reviews 14 (2010) 2611–2625. doi:10.1016/j.rser.2010.07.069.

[19] S. Chen, F. Witte, O. Kolditz, H. Shao, Shifted thermal extraction rates in large Borehole Heat Exchanger array – A numerical experiment, Applied Thermal Engineering 167 (2020) 114750. doi:10.1016/j.applthermaleng.2019.114750.

[20] T. You, X. Li, S. Cao, H. Yang, Soil thermal imbalance of ground source heat pump systems with spiral-coil energy pile groups under seepage conditions and various influential factors, Energy Conversion

and Management 178 (2018) 123–136. doi:10.1016/j.enconman.2018.10.027.

[21] K. W. Tordrup, S. E. Poulsen, H. Bjørn, An improved method for upscaling borehole thermal energy storage using inverse finite element modelling, Renewable Energy 105 (2017) 13–21. doi:10.1016/j.renene.2016.12.011.

[22] T. You, W. Wu, W. Shi, B. Wang, X. Li, An overview of the problems and solutions of soil thermal imbalance of ground-coupled heat pumps in cold regions, Applied Energy 177 (2016) 515–536. doi:10.1016/j.apenergy.2016.05.115.

[23] W. Choi, R. Ooka, Y. Nam, Impact of long-term operation of ground-source heat pump on subsurface thermal state in urban areas, Sustainable Cities and Society 38 (2018) 429–439. doi:10.1016/j.scs.2017.12.036.

[24] M. Saaly, P. Maghoul, M. Kavgic, D. Polyzois, Performance analysis of a proposed geothermal pile system for heating and cooling energy demand for a building in cold regions, Sustainable Cities and Society 45 (2019) 669–682. doi:10.1016/j.scs.2018.12.014.

[25] S. S. Naicker, S. J. Rees, Long-term high frequency monitoring of a large borehole heat exchanger array, Renewable Energy 145 (2020) 1528–1542. doi:10.1016/j.renene.2019.07.008.

[26] S. S. Naicker, Performance analysis of a large-scale ground source heat pump system, Ph.D. thesis, De Montfort University Leicester, 2015.

[27] S. S. Naicker, S. J. Rees, Performance analysis of a large geothermal heating and cooling system, Renewable Energy 122 (2018) 429–442. doi:10.1016/j.renene.2018.01.099.

[28] S. S. Naicker, S. J. Rees, Geothermal heat pump system operational data: high frequency monitoring of a large university building, University of Leeds, 2017. doi:10.5518/255.

[29] S. Koohi-Fayegh, M. A. Rosen, Examination of thermal interaction of multiple vertical ground heat exchangers, Applied Energy 97 (2012) 962–969. doi:10.1016/j.apenergy.2012.02.018.

[30] P. Hein, O. Kolditz, U. J. Görke, A. Bucher, H. Shao, A numerical study on the sustainability and efficiency of borehole heat exchanger coupled ground source heat pump systems, Applied Thermal Engineering 100 (2016) 421–433. doi:10.1016/j.applthermaleng.2016.02.039.

[31] A. Nguyen, P. Pasquier, D. Marcotte, Geothermics Borehole thermal energy storage systems under the influence of groundwater flow and time-varying surface temperature, Geothermics 66 (2017) 110–118. doi:10.1016/j.geothermics.2016.11.002.

[32] C. Chen, H. Shao, D. Naumov, Y. Kong, K. Tu, O. Kolditz, Numerical investigation on the performance, sustainability, and efficiency of the deep borehole heat exchanger system for building heating, Geothermal Energy 7 (2019) 18. doi:10.1186/s40517-019-0133-8.

[33] S. Pan, Y. Kong, C. Chen, Z. Pang, J. Wang, Optimization of the utilization of deep borehole heat exchangers, Geothermal Energy 8 (2020) 6. doi:10.1186/s40517-020-0161-4.

[34] R. Al-Khoury, T. Kölbel, R. Schramedei, Efficient numerical modeling of borehole heat exchangers, Computers & Geosciences 36 (2010) 1301–1315. doi:10.1016/j.cageo.2009.12.010.

[35] H.-J. Diersch, D. Bauer, W. Heidemann, W. Rühaak, P. Schätzl, Finite element modeling of borehole heat exchanger systems: Part 1. fundamentals, Computers & Geosciences 37 (2011) 1122–1135. doi:10.1016/j.cageo.2010.08.003.

[36] H.-J. Diersch, D. Bauer, W. Heidemann, W. Rühaak, P. Schätzl, Finite element modeling of borehole heat exchanger systems: Part 2. numerical simulation, Computers & Geosciences 37 (2011) 1136–1147. doi:10.1016/j.cageo.2010.08.002.

[37] F. Witte, I. Tuschy, TESPy: Thermal Engineering Systems in Python, Journal of Open Source Software 5 (2020) 2178. doi:10.21105/joss.02178.

[38] L. Bilke, H. Shao, S. Chen, W. Cai, OpenGeoSys Tutorial, Website, 2020. https://www.opengeosys.org/docs/userguide/basics/introduction/.

[39] H. M. Haq, E. Hiltunen, An inquiry of ground heat storage: Analysis of experimental measurements and optimization of system's perfor-

mance, Applied Thermal Engineering 148 (2019) 10–21. doi:10.1016/j.applthermaleng.2018.11.029.

[40] P. Bayer, M. de Paly, M. Beck, Strategic optimization of borehole heat exchanger field for seasonal geothermal heating and cooling, Applied Energy 136 (2014) 445–453. doi:10.1016/j.apenergy.2014.09.029.

[41] B. Meng, T. Vienken, O. Kolditz, H. Shao, Evaluating the thermal impacts and sustainability of intensive shallow geothermal utilization on a neighborhood scale: Lessons learned from a case study, Energy Conversion and Management 199 (2019) 111913. doi:10.1016/j.enconman.2019.111913.